

Phase-Averaged Gamma-Ray Spectra from Rotation-Powered Millisecond Pulsars

Z. J. Jiang,^{1,2} S. B. Chen,^{1,3} X. Li,¹ and L. Zhang^{1*}

¹*Department of Physics, Yunnan University, Kunming, 650091 China*

²*Yunnan Observatories, Chinese Academy of Sciences, Kunming, 650011 China*

³*Department of Physical Science and Technology, Kunming University, Kunming, 650214 China*

3 July 2018

ABSTRACT

Fermi-LAT has detected pulsed gamma-ray emissions with high confidences from more than 40 millisecond pulsars (MSPs). Here we study the phase-averaged gamma-ray properties of MSPs by using revised version of a self-consistent outer gap model. In this model, a strong multipole magnetic field near the stellar surface for a MSP is assumed and such a field will be close to the surface magnetic fields ($\sim 10^{11} - 10^{12}$ G) of young pulsars; the outer gap of a MSP is controlled by photon-photon pair production process, where the effects of magnetic inclination angle (α) and magnetic geometry have been taken into account, therefore the fractional size of the outer gap is a function of not only pulsar's period and magnetic field strength but also magnetic inclination angle and radial distance to the neutron star, the inner boundary of the outer gap can be estimated by the pair production process of the gamma-ray photons which are produced by the back-flowing particles through the null charge surface; inside the outer gap, a Gaussian distribution of the parallel electric field along the trans-field thickness is assumed, and the gamma-ray emission is represented by the emission from the average radial distance along the central field lines of the outer gap. Using this model, the phase-averaged gamma-ray spectra are calculated and compared with the observed spectra of 37 MSPs given by the second *Fermi*-LAT catalog of gamma-ray pulsars, our results show that the *Fermi*-LAT results can be well explained by this model. The thermal X-ray emission properties from MSPs are also investigated.

Key words: gamma rays: theory—pulsars: general—radiation mechanisms: non-thermal

1 INTRODUCTION

It is believed that millisecond pulsars (MSPs) are recycled neutron stars which spin up by accreting mass from their companions. MSPs are characterized by shorter spin periods ($P < 30$ ms) and smaller spin-down rates ($\dot{P} < 10^{-17}$ s s⁻¹) compared to the non-recycled young pulsars, indicating lower values of surface dipole magnetic field strengths and lower spin-down powers. Although these objects had been studied extensively at radio wavelength, it was not clear whether MSPs could produce gamma-rays like those of young pulsars before the launch of *Fermi Gamma-ray Space Telescope*.

The second *Fermi* Large Area Telescope (LAT) catalog of 117 γ -ray pulsars with high-confidences has been published recently (Abdo et al. 2013), which consists of 77 (42 radio-loud and 35 radio-quiet) young or middle-aged γ -ray pulsars and 40 millisecond γ -ray pulsars. Therefore, MSPs have become an important class of GeV objects, but the origin of gamma-ray photons from MSPs is still debated. From the *Fermi*-LAT observations of the MSPs (e.g., Abdo et al. 2013), the observed spectra can be fitted by a power law with an exponential cut-off, where the spectral index and the cut-off energy changes with the MSPs. Compared to young pulsars, it has been found that the MSPs share the same properties with young pulsars, so the gamma-ray emission mechanism for MSPs is similar with those of young pulsars.

* E-mail: lizhang@ynu.edu.cn

For either a young pulsar or a MSP, it is generally believed that the plasma with a charge density $\rho_{GJ} \approx -\vec{\Omega} \cdot \vec{B}/2\pi c$ (Goldreich & Julian 1969) will surround a rotating neutron star (NS) with an angular velocity Ω and co-rotate with the NS within the light cylinder with a radius $R_L = c/\Omega$. The global flow of plasma in the pulsar magnetosphere will result in charge depletion regions (called as gaps) in the open field line regions. Inside a gap, a strong electric field which is parallel to the magnetic field (called as an accelerating electric field or a parallel electric field) can be produced, the accelerating electric field will accelerate charged particles to relativistic energies and then produce gamma-ray emission through synchrotron radiation, curvature radiation and inverse Compton scattering from lower-energy photons. Due to different accelerating regions, various models have been proposed to explain the pulsed gamma-ray emission from young pulsars, for examples, polar cap model (e.g., Ruderman & Sutherland 1975; Daugherty & Harding 1982), slot gap model, (e.g., Arons 1983; Muslimov & Harding 2003, 2004; Harding et al. 2008), annular gap model (e.g., Qiao et al. 2004; Du et al. 2009), and outer gap model (e.g., Cheng et al. 1986a,b; Romani 1996; Zhang & Cheng 1997; Zhang et al. 2004; Zhang & Li 2009; Hirovani 2013; Li et al. 2013). For the high energy emissions from the MSPs, different models have also been proposed, such as annular gap model (Du et al. 2010, 2013), outer gap model (Takata et al. 2012), two layer outer gap model (Wang et al. 2010), and the emission geometry of MSPs has been studied by using the light curve from *Fermi*-LAT (Venter et al. 2009, 2012). It should be noted that current observations by the *Fermi*-LAT tend to favor the models in which gamma rays are generated in the outer magnetosphere (Abdo et al. 2010a,b). Therefore we will focus on the outer gap model for high energy emissions from the MSPs in this paper.

Compared to young pulsars, MSPs have shorter spin periods and smaller surface dipole magnetic fields. As suggested by Zhang & Cheng (2003), if there is only a dipole magnetic field in the magnetosphere of the MSP, then it is difficult to create the outer gap to accelerate e^\pm pairs to relativistic energy in the outer gaps. Therefore, Zhang & Cheng (2003) assumed that a strong multipole magnetic field exists near the stellar surface of the NS although a global dipole magnetic field can describe the magnetic field far from the star well. In this case, thermal X-rays are produced by the outer gap heating NS surface, and will collide with high energy gamma-rays produced in the outer gap through curvature radiation inside the outer gap, producing enough e^\pm pairs to sustain steady outer gaps. In the self-sustained outer gap model of Zhang & Cheng (2003), however, they did not consider the effects of the magnetic inclination angle and magnetic geometry and assumed that the typical radiation region locates at half of the light cylinder ($R_L/2$). Zhang et al. (2007) revised the model of Zhang & Cheng (2003) by taking the effects of the inclination angle and the magnetic geometry into account, and found that the fractional size of outer gap is a function not only of the pulsar period and magnetic field but also of the radial distance to the NS and the inclination angle. Zhang et al. (2007) also assumed that the average properties of high-energy photon emission from the outer gap can be approximated by the radiation at an average radius.

Recently, Li et al. (2013) described a revised version of the outer gap for explaining γ -ray properties of young γ -ray pulsars. In this outer gap model, an outer gap exists in the open field line region, where the lower boundary along the trans-field direction is in the last open field lines and the upper boundary is constrained by the photon-photon pair production process or critical field lines which are perpendicular to the rotational axis at the light cylinder, resulting in two possible types of outer gaps for the young pulsars, and the vertical distribution of the parallel electric field can be approximated as a Gaussian distribution (see details in Li et al. (2013) or references therein). Using this model, Li et al. (2013) reproduced the observed phase-averaged spectra of young gamma-ray pulsars. In this paper, we construct a revised model of the outer gap for studying the phase-averaged properties of gamma-ray emission from MSPs. The paper is organized as follows. In Section 2, we describe the details of the revised model. In Section 3, we apply the outer gap model to fit the phase-averaged gamma-ray emission and study the gamma-ray properties of MSPs. In Section 4, we give a brief conclusions and discussions.

2 MODEL DESCRIPTION

As mentioned above, the observations indicate that high-energy properties of the MSPs are similar to those of young pulsars, so we believe that some features of the outer gap model for young pulsars given by Li et al. (2013) can be also used to describe high energy emissions from the MSPs. In this paper, we will assume that the shape of the outer gap for a young pulsar described by Li et al. (2013) is also available for a MSP. Below we describe the details of the outer gap model used in this paper.

2.1 Accelerating Electric Field and Thermal X-Rays from Outer Gap Heating

The issue of the accelerating electric field inside the outer gap is a complicated issue. In the classic outer gap model (or vacuum outer gap model) (Cheng et al. 1986b), the outer gap is assumed to be thin and to extend from the null charge surface to the light cylinder. In such a gap, the accelerating electric field has a distribution along the direction of the gap height (or trans-field direction). If $h(r)$ and z represent the local thickness of the outer gap and a variable along the trans-field direction, respectively, Cheng et al. (1986b) demonstrated that the accelerating electric field is proportional to $q(1-q)$ and reaches a maximum at $q = 1/2$, where $q = z/h(r)$. On the other hand, the variations of the accelerating electric field along the direction

of the magnetic fields for young pulsars have been investigated by self-consistently solving the Poisson equation for electrical potential, and the Boltzmann equations of electrons/positrons, and gamma-rays in both vacuum and nonvacuum outer gaps (e.g., Hirovani & Shibata 1999; Takata et al. 2006; Lin et al. 2009).

According to Cheng et al. (1986b), Zhang & Cheng (1997) used the maximum accelerating electric field in the vacuum dipole magnetic field as the approximation of the accelerating electric field at position (r, θ) , where r is the radial distance to the star and θ is the polar angle. This accelerating electric field at position (r, θ) which is above the null charge surface can be approximated as (e.g., Zhang & Cheng 1997; Zhang et al. 2004)

$$E_{\parallel\max}(r, \theta) = f_m^2(r)B(r, \theta) \left(\frac{s}{R_L} \right) \quad \text{for } r_n \leq r \leq r_{\text{out}}, \quad (1)$$

where $f_m(r) \equiv h(r)/R_L$ is the fractional size of outer gap, s is the local curvature radius, R_L is the radius of the light cylinder, and $B(r, \theta)$ is the dipole magnetic field strength at the position (r, θ) . In Eq. (1), r_n is the radial distance of the null charge surface and corresponding polar angle is $\theta_n = \tan^{-1}[(3 \tan \alpha + \sqrt{8 + 9 \tan^2 \alpha})/2]$. Below the null charge surface, the accelerating electric field below the null charge surface can be approximated by (e.g., Tang et al. 2008; Zhang & Li 2009)

$$E_{\parallel\max}^{\text{in}} = E_{\parallel\max}(r_n, \theta_n) \frac{(r/r_{\text{in}})^2 - 1}{(r_n/r_{\text{in}})^2 - 1} \quad \text{for } r_{\text{in}} \leq r < r_n, \quad (2)$$

where r_{in} is the radial distance of the inner boundary (see Eq. (9) of Li et al. (2013)).

Since the maximum accelerating electric field locates at the center of the gap height for a given position (r, θ) , so we can choose the magnetic field lines which cross the center of the gap height as typical field lines of accelerating particle and then emitting gamma-rays, i.e., the accelerating electric field at any position (r, θ) of the typical field line being tangent to the light cylinder with a radius of $R'_L = \kappa R_L$ ($\kappa \geq 1$) is given by Eq. (1). In this case, we can use a Gaussian distribution to approximate the distribution of the accelerating electric field along the trans-field direction given by Li et al. (2013), which is

$$E_{\parallel p}(q) = \frac{E_{\parallel\max} - E_{\parallel\min}}{1 - e^{-\frac{1}{2}0.5^2/\sigma_g^2}} \times \left[e^{-\frac{(q-0.5)^2}{2\sigma_g^2}} + \frac{E_{\parallel\min} - e^{-\frac{1}{2}0.5^2/\sigma_g^2} E_{\parallel\max}}{E_{\parallel\max} - E_{\parallel\min}} \right], \quad (3)$$

where $q = z/h(r)$, $E_{\parallel\min} = (2/3)(e/R_L^2)(s/R_L)^{-2}$ is the minimum value of the accelerating field line along the trans-field direction, and σ_g is the standard deviation of the Gaussian distribution which is treated as a model parameter (Li et al. 2013).

We now consider the thermal X-rays from the outer gap heating. In the self-sustained outer gap model (Zhang & Cheng 2003; Zhang et al. 2007), the local magnetic field will dominate over the global dipole field in the region R to $R + \delta r$, but the magnetic field can be described by the dipole field in the region $r > R + \delta r$, where δr is the distance above the stellar surface in which the local magnetic field is equal to the dipole magnetic field and R is NS radius. Assuming a localized dipole field form of the local magnetic field, the relationship between the local field and the dipole field can be expressed as $B_s^0/B_d^0 = [(R + \delta r)/R]^{-3}[(l + \delta r)/l]^3$ (e.g., Zhang & Cheng 2003), where $B_d^0 = 3.2 \times 10^{19} (P\dot{P})^{0.5}$ G is the dipole magnetic field at the stellar surface, and l is the typical radius of curvature of the local magnetic field with a surface strength B_s^0 . In such a case, Zhang & Cheng (2003) and Zhang et al. (2007) investigated the thermal X-ray production caused by the back-flowing particles from the outer gap (also see Takata et al. 2012). The return particle flux can be approximated by $\dot{N}_{e\pm} \simeq 0.5f(r_{\text{in}})\dot{N}_{\text{GJ}}$, where $f(r_{\text{in}})$ is the fractional size of the outer gap in the inner boundary and \dot{N}_{GJ} is the Goldreich-Julian current. Those particles loss energies via curvature radiation and the remaining energy can be approximated as $E(R + \delta r) = m_e c^2 \gamma(R + \delta r)$ when reaching the distance $R + \delta r$, and $E(R) = m_e c^2 \gamma(R)$ when reaching the NS surface. In the region between $R < r < R + \delta r$, the local magnetic field dominate the global dipole field, and the curvature photons will convert into e^\pm pairs in the strong local magnetic field, and finally deposit on the NS surface with an effective area $A_{\text{eff}}^{(1)} \simeq \pi(\delta r)^2$ and produce the first component of thermal X-ray emission, and the luminosity can be approximated as $L_X^{\text{th1}} \simeq 0.5m_e c^2 [\gamma(R + \delta r) - \gamma(R)]\dot{N}_{e\pm}$, and the temperature can be expressed as $T_m^{(1)} = (L_X^{\text{th1}}/A_{\text{eff}}^{(1)}\sigma_{\text{SB}})^{1/4}$, which is given by equation (11) of Zhang et al. (2007). The second component of thermal X-rays is produced by the back-flowing particle with energy $E(R) = m_e c^2 \gamma(R)$ deposited on an effective area $A_{\text{eff}}^{(2)} \simeq (B_d^0/B_s^0)\pi r_{\text{pc}}^2$ with thermal luminosity $L_X^{\text{th1}} \simeq m_e c^2 \gamma(R)\dot{N}_{e\pm}$ and temperature $T_m^{(2)}$ which is given by equation (13) of Zhang et al. (2007).

2.2 The Fractional Size of the Outer Gap

The thermal X-ray photons with energy $< E_X \gg 2.7kT_m^{(1)}$ will collide with the curvature gamma-ray photons with energy E_γ given by equation (7) of Zhang et al. (2007) to produce enough e^\pm to sustain a steady outer gap, where k is the Boltzmann constant. With photon-photon pair production condition, Zhang et al. (2007) derived the expression of the fractional size of the outer gap above the null charge surface, which is

$$f_m(r, \alpha) \approx 5.9 \times 10^{-2} P_{\text{ms}}^{26/21} \left(\frac{B_d^0}{10^8 \text{ G}} \right)^{-4/7} \delta r_5^{2/7} \eta(\alpha, r) \quad \text{for } r_n \leq r \leq r_{\text{out}}, \quad (4)$$

where P_{ms} is the pulsar period in units of millisecond, B_d^0 is dipole magnetic field at stellar surface in units of Gauss, $\delta r_5 = \delta r/10^5$ cm, and the function $\eta(r, \alpha)$ contains the effects of inclination angle and magnetic geometry, and can be estimated by using Eqs. (17) - (20) of Zhang et al. (2007). The distance δr , where the local magnetic field is equal to the dipole magnetic field, can be estimated as $\delta r = l[(B_s^0/B_d^0)^{1/3} - 1]/[1 - (l/R)(B_s^0/B_d^0)^{1/3}]$. We can see that δr depends on l and B_s^0/B_d^0 , both of them are still unclear. Generally, it is assumed that the curvature radius l of the local magnetic field is of the order of the crust thickness of the star, $l \sim 10^5$ cm, and $B_s^0 \sim 10 - 10^3 B_d^0$ (e.g., Ruderman 1991; Chen et al. 1998). In our following calculation, we assume that $l = 0.5 \times 10^5$ cm, $B_s^0/B_d^0 = 300$ and $R=12$ km as taken by Zhang et al. (2007), then we have $\delta r_5 \sim 4$.

In the region from the inner boundary to the null charge surface, the fractional size of the outer gap can be estimated by using the magnetic flux conservation in the outer gap (e.g., Zhang & Li 2009), i.e., $f_m^{\text{in}}(r, \alpha) = f_m(r_n, \alpha)[B(r_n, \theta_n)/B(r, \theta)]^{1/2}$ for $r_{\text{in}} \leq r \leq r_n$.

2.3 Phase-Averaged Gamma-Ray Spectrum

In this section, we consider the phase-averaged spectrum of gamma-ray emission from a MSP. Zhang & Cheng (2003) (also see Zhang et al. (2007)) did not consider the accelerating electric field along the trans-field direction and assumed the accelerating electric field along a specific magnetic field line near the last open field line as typical one for simplicity. Different from Zhang et al. (2007), in this paper, the typical field line is the field line which is tangent to the light cylinder with a radius of $R_L' = \kappa R_L$. Moreover we assume that high-energy emission at an average radius r_a along the typical field line can represent the typical emission of high-energy photons from a MSP and the average radius over the entire outer gap is given by

$$r_a = \frac{\int_{r_{\text{in}}}^{r_{\text{out}}} f_m(r, \alpha) r dr}{\int_{r_{\text{in}}}^{r_{\text{out}}} f_m(r, \alpha) dr}, \quad (5)$$

where $r_{\text{out}} = \min(r_b, r_{\text{LC}})$.

We assume that gamma-rays from a MSP are mainly produced by the curvature radiation of the accelerated particles and the gamma-ray beam points toward the observer. Therefore, the phase-averaged gamma-ray spectrum of a young pulsar given by Li et al. (2013) can also be used to describe that of a MSP. In this case, the phase-averaged gamma-ray spectrum can be estimated as (Li et al. 2013):

$$F_\gamma^{\text{th}}(E_\gamma) \approx \left(\frac{\Delta\phi}{\Delta\Omega} \right) \frac{f_g^3(r_a, \alpha) L_{\text{sd}}}{E_\gamma d^2} U(x) \left(\frac{r_a}{R_L} \right)^{-4}, \quad (6)$$

where d is the distance to the pulsar, (r_a, θ_a) represents the typical radiation position, $\Delta\phi$ is the extension angle at azimuthal direction, $\Delta\Omega$ is the gamma-ray beaming solid angle, $L_{\text{sd}} \approx 3.8 \times 10^{35} (P/\text{ms})^{-4} (B_d^0/10^8 \text{ G})^2$ erg/s is the spin down power of a pulsar, and the function $U(x)$ is given by Eq. (22) of Li et al. (2013).

For comparison with the observed cutoff energy of a MSP's SED, we give the characteristic energy of the curvature photons, which is

$$E_\gamma(r_a) \approx 4.3 \times 10^{10} f_m^{3/2}(r_a) \left(\frac{B_d^0}{10^8 \text{ G}} \right)^{3/4} P_{\text{ms}}^{-7/4} \left(1 - \frac{3}{4} \frac{a(\alpha) r_a}{R_L} \right)^{3/8} \left(\frac{r_a}{R_L} \right)^{-13/8} W^{-1/4}(r_a, \alpha) \text{ eV}, \quad (7)$$

where $P_{\text{ms}} = P/1$ ms, and $W(r_a, \alpha) = s/\sqrt{r_a R_L} = (4/3)[1 - (3/4)a(\alpha)(r_a/R_L)]^{3/2}/[\sqrt{a(\alpha)}(1 - (1/2)a(\alpha)r_a/R_L)]$ with $a(\alpha) = \sin \theta_{\text{LC}} \sin^2(\theta_{\text{LC}} - \alpha)$.

3 APPLICATIONS

We now apply the above outer gap model to study the phase-averaged gamma-ray spectra from MSPs. In the second *Fermi*-LAT catalog of gamma-ray pulsars, there are 40 gamma-ray MSPs and the spectral fitting results by using an exponentially cut-off power-law are presented, and the observed spectral energy distributions (SEDs) of these MSPs except for three of them (PSRs J1024-0719, J1741+1351 and J1939+2134) are also presented. Here we compare the model results with observed SEDs of 37 MSPs. The periods, surface magnetic field and distances of these MSPs are listed in Table 1, which will be used in our calculations.

For a pulsar with known period and period derivative, if the inclination angle α is given, we can estimate the fractional size of the outer gap, and then calculate the gamma-ray SED. In fact, observationally it is difficult to obtain the value of inclination angle, so we treat α as a model parameter which can be determined by fitting the observed gamma-ray spectrum. Two other parameters in our calculations are the extension at azimuthal direction $\Delta\phi$ and beaming solid angle $\Delta\Omega$. $\Delta\phi$ can

be estimated by the pair production, and $\Delta\Omega = 4\pi f_\Omega$, where f_Ω is the gamma-ray beaming fraction, which depends on the inclination angle, viewing angle and the detail structure of the outer gap (Watters et al. 2009), and the pulsar beaming model indicated that $f_\Omega \sim 1$. In this paper, we do not consider the specific value of f_Ω for each pulsar, we combine $\Delta\phi$ and $\Delta\Omega$ as a single model parameter $\frac{\Delta\phi}{\Delta\Omega}$ because $F_\gamma^{\text{th}}(E_\gamma) \propto (\Delta\phi/\Delta\Omega)$ (see Eq. (6)). Therefore, for a given MSP, i.e., its rotation period, period derivative and distance to the Earth are given, the model has three parameters: α , $\Delta\phi/\Delta\Omega$, and σ_g .

We use the outer gap model to reproduce the phase-averaged gamma-ray spectra of MSPs observed by *Fermi*-LAT. In order to determine the best model parameters, the chi-square goodness of fit test is used, the chi-square test statistic can be written as

$$\chi^2 = \sum_i \frac{[F_\gamma^{\text{ob}}(E_\gamma) - F_\gamma^{\text{th}}(E_\gamma)]^2}{\sigma^2(E_\gamma)}, \quad (8)$$

where $F_\gamma^{\text{th}}(E_\gamma)$ is the model flux given by equation (6), $F_\gamma^{\text{ob}}(E_\gamma)$ is the observed flux, and $\sigma(E_\gamma)$ is the corresponding error, the observed data are taken from the second *Fermi*-LAT catalog of gamma-ray pulsars (Abdo et al. 2013).

We fit the observed spectra as follows. First, we use a specific value of α to estimate the fractional size $f_g(r, \alpha)$, then estimate the averaged radius r_a by equation (5), and the corresponding fractional size $f(r_a, \alpha)$. Second, we obtain an electronic field distribution by equation (3) with a specific value of σ_g . As proposed by Li et al. (2013), σ_g increases with the fractional size $f_g(r_a, \alpha)$. It is reasonable to assume that σ_g is larger for a pulsar with thick outer gap than one with thin outer gap. In our following calculation, for simplicity, we assume $\sigma_g = 0.15$ when $f_g(r_a, \alpha) < 0.2$, $\sigma_g = 0.2$ when $0.2 \leq f_g(r_a, \alpha) < 0.3$, $\sigma_g = 0.25$ when $0.3 \leq f(r_a, \alpha) < 0.4$, and $\sigma_g = 0.3$ when $f_g(r_a, \alpha) > 0.4$. As shown in our following calculations, the above assumption about σ_g is a good approximation. Third, we calculate the gamma-ray spectrum at typical radius r_a by equation (6) and compare it with the observation to find the best fitting results of $\Delta\phi/\Delta\Omega$. It should be noted that, the slope of the calculated spectrum is mainly controlled by α and σ_g , and the magnitude can be modified by $\Delta\phi/\Delta\Omega$. So for a given α and σ_g , we change the value $\Delta\phi/\Delta\Omega$ to get a minimum value of χ^2 by equation (8). Finally, we change the values of α to repeat above processes to obtain the minimum of χ^2 , then we can obtain the best fitting parameters of α and $\Delta\phi/\Delta\Omega$, and the reduced chi-square, χ^2/ν , where $\nu = N - 2$ is the degree of freedom and N is the number of observed data.

The best fitting parameters are presented in Table 1, which include the inclination angle α and $\Delta\phi/\Delta\Omega$. We can see that the inclination angles for $\sim 80\%$ MSPs are larger than the 60° . In our model, larger value of the inclination angle for a given MSP means larger value of the γ -ray typical energy. For the best fits of the parameter $\Delta\phi/\Delta\Omega$, change range is very large, from ~ 0.02 to ~ 2.8 , 7 of 33 MSPs have $\Delta\phi/\Delta\Omega > 1$ which seems not to be reasonable. By definition, $\Delta\phi$ is the extension angle of the outer gap at the azimuthal direction and could be less than 2π and $\Delta\phi \sim 250^\circ$ for most of young pulsars (Li et al. 2013), $\Delta\Omega$ is the solid angle of γ -ray beam, according to Watters et al. (2009), the gamma-ray beaming fraction $f_\Omega \sim 1$ for most young γ -ray pulsars, which means $\Delta\Omega \sim 4\pi$. Therefore, $\Delta\phi/\Delta\Omega \sim 0.35$ for a MSP with $\Delta\phi \sim 250^\circ$ and $\Delta\Omega \sim 4\pi$. However, as shown in Table 1, there are large differences among the fitting value of $\Delta\phi/\Delta\Omega$, which may be caused by the the uncertainties of distances and the geometry of outer gaps. In fact, the inclination angle and $\Delta\Omega$ for a given MSP can be estimated by reproducing its high-quality γ -ray light curve in the frame of some three-dimensional (3D) model (for example outer gap (OG) model, or two-pole caustic (TPC) model), Watters et al. (2009) calculated the beaming patterns and light curves of young γ -ray pulsars in both TPC and OG models and found that γ -ray light curve shapes depend sensitively on α and viewing angle ζ . Venter et al. (2009) computed the γ -ray beaming patterns and light curves of MSPs in both TPC and OG models and compared calculation results with those observed by *Fermi*-LAT, they gave the values of α and f_Ω for 7 MSPs (see Table 3 of Venter et al. (2009)). Compared to our results, the differences are obvious.

In Table 1, we list the values of the averaged radius r_a and the coefficient κ for each MSP. We can see that the values of r_a for most MSPs are close to 1, indicating typical emissions occur near outer magnetosphere. On the other hand, the values of κ changes from ~ 1.2 to ~ 2.0 , showing that the curvature radiation regions for most MSPs are close to the null charge surface. In this table, the fractional size f_m estimated by equation (4) are also listed.

The comparisons of model SEDs with the best fitting parameters with observed ones for 37 MSPs are shown in Fig. 1 and Fig. 2. Although the observed SEDs of 37 MSPs are available, the observed data are poor for some MSPs. Using a power law with an exponential cutoff, i.e. $F_\gamma^{\text{ob}}(E_\gamma) \propto E^{-\Gamma} \exp(-E/E_{\text{cut}})$, where Γ is the spectral index and E_{cut} is the cutoff energy, Abdo et al. (2013) have given the best-fit values of Γ , E_{cut} and $F_\gamma^{\text{ob}}(E_\gamma)$. In order to compare our results with the observed data better, we also show the best fits (blue lines) with one σ uncertainties (red dashed lines) by using a power law with an exponential cutoff given by Abdo et al. (2013). In Fig. 1 and Fig. 2, our best fitting model spectra with the fitting parameters listed in Table 1 are shown with the black solid lines, the data points are the observed data from the *Fermi*-LAT, which are taken from Abdo et al. (2013). We can see that the outer gap model can well explain the observations of most of MSPs, and the fitted χ^2/ν also indicate that the model results are consistent with the observations. As shown in Fig. 1 and Fig. 2, however, 8 of 37 MSPs have large values of $\chi^2/\nu > 10$, we believe that these large values are mainly caused by the limited observation data. For example, there are only 6 data points (including 3 upper limits) for J1658-5324, resulting in $\chi^2/\nu \approx 63$, same case is for J1648-5324; for J2047+1053, 7 data points include 6 upper limits, resulting in $\chi^2/\nu \approx 53$. Although large χ^2/ν for these MSPs, our model results can compare with the best fits by using a power law with an exponential cutoff. On

the other hand, from Fig. 1, Fig. 2, and Table 1, 5 MSPs (J1514-4946, J1614-2230, J2043+1711, J2124-3358, and J2302+4442) with better data points have χ^2/ν values from ~ 5 to ~ 9 . The differences between our model results with the data points can be divided two cases: the first case is that our results cannot fit the data points at low energy part (J1514-4946 and J2043+1711), implying that some radiation mechanism may have a role in the low energy part; the second case is that our results cannot fit the data points at peak energy range of E^2F (J1614-2230, J2124-3358, and J2302+4442). In fact, if we relax the limit of σ_g (see above), our results can fit the data points well for the second case.

It should be noted the gamma-ray spectral properties of PSR J0218+4232. This pulsar has high X-ray luminosity, hard power-law shaped X-ray spectra and emits narrow X-ray pulse, Kuiper et al. (2000) reported the likely detection of pulsed gamma-ray emission from this pulsar using CGRO EGRET data and found that the X-ray and gamma-ray pulse profile shapes (doubled peaks) are similar. Since PSR J0218+4232 and Crab pulsar have the similarities of high energy pulse profiles and have that the magnetic field strengths near the light cylinders are comparable, Kuiper et al. (2000) pointed out that pulsed high-energy nonthermal emission from PSR J0218+4232 and Crab pulsar have a similar origin in the pulsar magnetosphere. However, the gamma-ray pulse profile observed by *Fermi*-LAT show a single pulse Abdo et al. (2013), which is not consistent with that given by Kuiper et al. (2000). For the Crab pulsar, the synchrotron-self Compton radiation process play an important role in the outer gap model (e.g., Zhang & Cheng 2002; Li & Zhang 2010). Here, we find that only curvature radiation cannot explain the observed SED of PSR J0218+4232 very well (see Fig. 1 and Table 1) and other radiation mechanisms seem to be required.

In the outer gap model, there are two components of thermal X-ray emission caused by heating of return particles from the outer gap. The observed thermal X-ray spectra of MSPs can be fitted by blackbody radiation with one or two temperatures. In Table 1, we list the observed temperatures $T_{m,o}^{(1)}$ and $T_{m,o}^{(2)}$ for each MSP if available from literatures, we also present the predicted temperatures $T_m^{(1)}$ and $T_m^{(2)}$ estimated by equations (11) and (13) of Zhang et al. (2007), respectively. We can see that $T_m^{(1)} \sim (0.5 - 0.8) \times 10^6$ K and $T_m^{(2)} \sim (1.5 - 4) \times 10^6$ K, which are roughly consistent with the observations. We also listed the observed thermal X-ray luminosities in the seventh column, which are estimated by $L_X^{(ob)} = 4\pi d^2 F_{BB}$, where F_{BB} is the unabsorbed X-ray flux, and the modeled thermal luminosities $L_X^{(th)}$ are listed in seventeenth column, which are estimated by equation (27) of (Zhang et al. 2007). We can see that the model results can roughly explain the observations, and the differences for some MSPs are likely caused by the limited observations or by the uncertainties of multipole field.

Finally, we compare model results of typical energy given by Eq. (7) with the values of E_{cut} given by Abdo et al. (2013). In this revised outer gap model, we have assumed that curvature photon emission at the position (r_a, θ_a) of the typical field line represents the typical emission of high energy γ -rays from a given MSP, so the characteristic energy estimated by Eq. (7) for each MSP would be a good approximation of observed E_{cut} because of the feature of the curvature radiation. In Fig. 3, we show the comparison of the model results with the observed E_{cut} given by Abdo et al. (2013), where dashed line represents $E_{cur} = E_{cut}$ and solid line is the fit result. We can see that the typical gamma-ray energy E_{cur} is comparable with E_{cut} , which satisfies the relation $E_{cut} = (0.37 \pm 0.27) + (0.77 \pm 0.12)E_{cur}$.

4 CONCLUSIONS AND DISCUSSION

We have studied the phase-averaged gamma-ray spectra from rotation-powered MSPs based on the revised outer gap model of Zhang et al. (2007). In this model, there is a strong multipole magnetic field near the stellar surface, and the back-flowing particles from the outer gap will finally convert into X-ray photons in this strong magnetic field, which can collide with the curvature gamma-ray photons in the outer gap and then produce electron/positron pairs to sustain a self-consistent outer gap, and the fractional size of the outer gap can be estimated by the pair production condition. In this revised outer gap model, the effects of the magnetic inclination angle and magnetic geometry have been taken into account, and the gamma-ray emission at an averaged radius can be used to represent the phase averaged gamma-ray emission. In this paper, we have made three assumptions for study of the gamma-ray emission from MSPs: (i) the gamma-ray emission along the central field lines in the outer gap can be used to represent the typical gamma-ray emission from MSPs, which is more reasonable than the assumption that the gamma-ray emission along the last open field lines represents the typical gamma-ray emission; (ii) the typical gamma-ray emission at the averaged radius r_a can be used to represent the whole gamma-ray emission from MSPs; (iii) the electric field in the trans-field direction of the outer gap can be represented by a Gaussian distribution, such an assumption has been successfully used to explain the gamma-ray emission from normal young pulsars (Li et al. 2013). With this model, we calculated the phase-averaged gamma-ray spectra of 37 MSPs given by the second *Fermi*-LAT catalogue of gamma-ray pulsars. The Chi-square goodness of fit test has been used to find the best fitting parameters for each MSP. The estimated phase-averaged gamma-ray spectra of these MSPs are presented in Figures 1 and 2, and the best fitting parameters are listed in Table 1. We can see that the revised outer gap model can well explain the observed phase-averaged gamma-ray spectra and thermal X-ray emission of most MSPs.

In this paper, we also estimated the inner boundary of outer gap. In the traditional outer gap model of gamma-ray pulsars, the inner boundary of the outer gap is assumed at the null-charge surface. However, Hirotani (2008) pointed out that

the inner boundary of the outer gap can be shifted inward from the null charge surface. Such a modification is important when the light curve and phase-resolved spectra of the normal pulsars is reproduced in the three dimensional outer gap models (e.g. Tang et al. 2008). In this work, we estimated the inner boundary of the outer gap of MSPs by the pair production process and found that such an improvement just causes marginal changes when the phase-averaged gamma-ray spectra is calculated. However, it could play an important role when the three dimensional out gap model of MSPs is constructed.

In our model, two parameters of α and $\Delta\phi/\Delta\Omega$ can be estimated by fitting the phase-averaged spectra of gamma-ray emissions from MSPs. These two parameters can also be estimated through simulating the light curve of a MSP observed by *Fermi*-LAT. Generally, the inclination angle is hard to measure directly and the simulation of the γ -ray light curve for a pulsar needs to be performed in a specific three-dimensional model. Simulated light curve depends on not only the inclination angle α and viewing angle ζ but also the models used. For example, Watters et al. (2009) simulated the γ -ray light curves for young pulsars in TPC and OG models, the values of α and ζ for a young pulsar can be different in different models (see their Table 1). Moreover, the flux correction factor f_Ω and then $\Delta\Omega$ are also different for various model. The same case occurs in the simulations of the γ -ray light curves of MSPs (Venter et al. 2009, 2012). Therefore, the values of α and $\Delta\Omega$ obtained from the simulations of the γ -ray light curves for γ -ray pulsars are still uncertain. Not only the magnetic inclination angle α , but also the viewing angle ζ are highly unknown. Thus, the flux correction factor (or equivalently $\Delta\phi/\Delta\Omega$ in this paper) is anyway highly unknown as well. There are 7 MSPs (out of total 37) with $\Delta\phi/\Delta\Omega > 1$ as listed in Table 1. This is probably because the flux correction factor becomes less than unity; that is, we are observing such MSPs from the direction toward which more gamma-rays are emitted from other directions.

In our model, the role of the parameter σ_g is to adjust the width of the accelerating electric field along the trans-field direction and then has a effect on the SED's shape: smaller value of σ_g results in a rise of the SED at low energy part for a MSP with a given α , vice versa. Our model indicate that the change of σ_g is from ~ 0.15 to ~ 0.30 .

It should be noted that the properties of the multipole magnetic field play important roles when estimate the fractional size f_m and the thermal X-ray temperatures $T_m^{(1)}$ and $T_m^{(2)}$, which are severely depend on the unclear parameters l and B_s^0/B_d^0 . For simplicity, we take $l = 0.5 \times 10^5$ cm and $B_s^0 = 300B_d^0$ for each MSP, which result in $\delta r_5 \simeq 3.95$. As shown by equation (4), $f_m \propto \delta r_5^{2/7}$, then the gamma-ray luminosity $L_\gamma \propto \delta r_5^{6/7}$. So different values of l and B_s^0/B_d^0 will affect the estimation about the gamma-ray luminosity, also influence the X-ray emission properties. For example, if $l = 1 \times 10^5$ cm and $B_s^0/B_d^0 = 100$ (Zhang & Cheng 2003), then $\delta r_5 \simeq 6.8$, which can cause the difference when estimated the gamma-ray luminosity. However, such uncertainty can be combined with uncertainty of the gamma-ray flux correction factor ($\delta\phi/\Delta\Omega$) mentioned above and unchange the main results in this paper.

Fermi-LAT second source catalog lists 575 unassociated sources which have no obvious counterparts at other wavelengths, some statistical methods have been used to analyze the origin of these unassociated sources (e.g., Ackermann et al. 2012). Generally speaking, most of the unassociated Galactic objects are likely related to pulsars, pulsar wind nebulae, and supernova remnants. Since these objects have pulsar-like spectra and variability characteristics, the deep radio observation have been performed and recognized more than 40 gamma-ray MSPs (e.g., Ray et al. 2012; Kerr et al. 2012; Keith et al. 2011; Ransom et al. 2011; Barr et al. 2013), These discoveries greatly increase the known population of MSPs, and the deep survey by radio telescope and multi-wavelength observations will find more MSPs, which will help us to improve our model.

ACKNOWLEDGMENTS

We thank the anonymous referee for his/her valuable comments. This work is partially supported by the National Natural Science Foundation of China (NSFC 11173020, 11363006) and Doctoral Fund of Ministry of Education of China (RFDP 20115301110005).

REFERENCES

- Abdo, A. A., Ackermann, M., Ajello, M., et al. 2009, *Science*, 325, 848
- Abdo, A. A., Ackermann, M., Ajello, M., et al. 2010a, *ApJS*, 187, 460
- Abdo, A. A., Ackermann, M., Ajello, M., et al. 2010b, *ApJ*, 712, 957
- Abdo, A. A., Ajello, M., Allafort, A., et al. 2013, arXiv: 1305.4385
- Ackermann, M., Ajello, M., Allafort, A., et al. 2012, *ApJ*, 753, 83
- Arons, J. 1983, *ApJ*, 266, 215
- Barr, E. D., Guillemot, L., Champion, D. J., et al. 2013, *MNRAS* 429, 1633
- Blandford, R. D., Applegate, J. H., & Hernquist, L. 1983, *MNRAS*, 204, 1025
- Bogdanov, S., & Grindlay, J. E. 2009, *ApJ*, 703, 1557
- Chen, K., Ruderman, M., & Zhu, T. 1998, *ApJ*, 493, 397
- Cheng, K. S., Ho, C., & Ruderman, M. 1986a, *ApJ*, 300, 500

- Cheng, K. S., Ho, C., & Ruderman, M. 1986b, *ApJ*, 300, 522
- Cheng, K. S., Ruderman, M. A., & Zhang, L. 2000 *ApJ*, 537, 964
- Cognard, I., Guillemot, L., Johnson, T. J., et al. 2011, *ApJ*, 732, 47
- Daugherty, J. K. & Harding, A. K. 1982, *ApJ*, 252, 337
- Du, Y. J., Xu, R. X., Qiao, G. J., & Han, J. L. 2009, *MNRAS*, 399, 1587
- Du, Y. J., Qiao, G. J., Han, J. L., et al. 2010, *MNRAS*, 406, 2671
- Du, Y. J., Qiao, G. J., & Chen, D. 2013, *ApJ*, 763, 29
- Fang, J., & Zhang, L. 2010, *ApJ*, 718, 467
- Gentile, P., Roberts, M., McLaughlin, M. et al., 2013, arXiv:1305.6799v1
- Goldreich, P. & Julian, W. H. 1969, *ApJ*, 157, 869
- Harding, A. K., Stern, J. V., Dyks, J. & Frackowiak, M. 2008, *ApJ*, 680, 1378
- Hessels, J. W. T., Roberts, M. S. E., McLaughlin, M. A., et al. 2011, *AIPC*, 1357, 40
- Hirovani, K., & Shibata, S. 1999, *MNRAS*, 308, 54
- Hirovani, K., 2008, *ApJ*, 688, L25
- Hirovani, K., 2013, *ApJ*, 766, 98
- Keith, M. J., Johnston, S., Ray, P. S., et al. 2011, *MNRAS*, 414, 1292
- Kerr, M., Camilo, F., Johnson, T. J., et al. 2012, *ApJ*, 748, L2
- Kuiper, L., Hermsen, W., Verbunt, F., et al. 2000, *A&A*, 359, 615
- Li, X., Jiang, Z. J. & Zhang, L. 2013, *ApJ*, 765, 124
- Li, X., & Zhang, L. 2010, *ApJ*, 725, 2225
- Lin, G. F., & Zhang, L. 2009, *ApJ*, 699, 1711
- Marelli, M. 2012, PhD thesis, arXiv:1205.1748v1
- Muslimov, A., and Harding, A. 2003, *ApJ*, 588, 430
- Muslimov, A. & Harding, A. K. 2004, *ApJ*, 606, 1143
- Nolan, P. et al. *Astroph. J Suppl.* 199, 31 (2012).
- Pancrazi, B., Webb, N. A., Becker, W., et al. 2012, *A&A*, 544, 108
- Qiao, G. J., Lee, K. J., Wang, H. G., Xu, R. X., & Han, J. L. 2004, *ApJ*, 606, L49
- Ransom, S. M., Ray, P. S., Camilo, F., et al. 2011, *ApJ*, 727, L16
- Ray, P. S., Abdo, A. A., Parent, D., et al. 2012, arXiv:1205.3089v1
- Romani, R. W. 1990, *Nature*, 347, 741
- Romani, R. 1996, *ApJ*, 470, 469
- Ruderman, M. A., & Sutherland, P. 1975, *ApJ*, 196, 51
- Ruderman, M. A. 1991, *ApJ*, 366, 261
- Takahashi, Y.; Kataoka, J. Nakamori, T. Maeda, K., et al. 2012, *ApJ*, 747, 64
- Takata, J., Shibata, S., Hirovani, K., & Chang, H.-K. 2006, *MNRAS*, 366, 1310
- Takata, J., & Chang, H.-K. 2007, *ApJ*, 670, 677
- Takata, J. & Chang, H. -K. 2009, *MNRAS*, 392, 400
- Takata, J., Cheng, K. S., & Taam, Ronald E. 2012, *ApJ*, 745, 100
- Tang, A. P. S., Takata, T., Jia, J. J., & Cheng, K. S. 2008, *ApJ*, 676, 562
- Venter, C., Harding, A. K., & Guillemot, L. 2009, *ApJ*, 707, 800
- Venter, C., Johnson, T. J., & Harding, A. K., 2012, *ApJ*, 744, 34
- Watters K. P., Romani R.W., Weltevrede P., Johnston S., 2009, *ApJ*, 695, 1289
- Wang, Ren-Bo, & Hirovani, K. 2011, *ApJ*, 736, 127
- Wang, Y., Takata, J., & Cheng, K. S. 2010, *ApJ*, 720, 178
- Webb, N. A., Olive, J.-F., & Barret, D. 2004, *A&A*, 417, 181
- Wu, J. H. K., Kong, A. K. H., Huang, R. H. H., et al., 2012, *ApJ*, 748, 141
- Zavlin, V. E., 2006, *ApJ*, 638, 951
- Zhang, L., & Cheng, K. S. 1997, *ApJ*, 487, 370
- Zhang, L., & Cheng, K. S. 2003, *A&A*, 398, 639
- Zhang, L., & Cheng, K. S. 2002, *ApJ*, 569, 872
- Zhang, L., Cheng, K. S., Jiang, Z. J., & Leung, P. 2004, *ApJ*, 604, 317
- Zhang, L., Fang, J. & Chen, S. B. 2007, *ApJ*, 666, 1165
- Zhang, L., & Li, X. 2009, *ApJ*, 707, L169

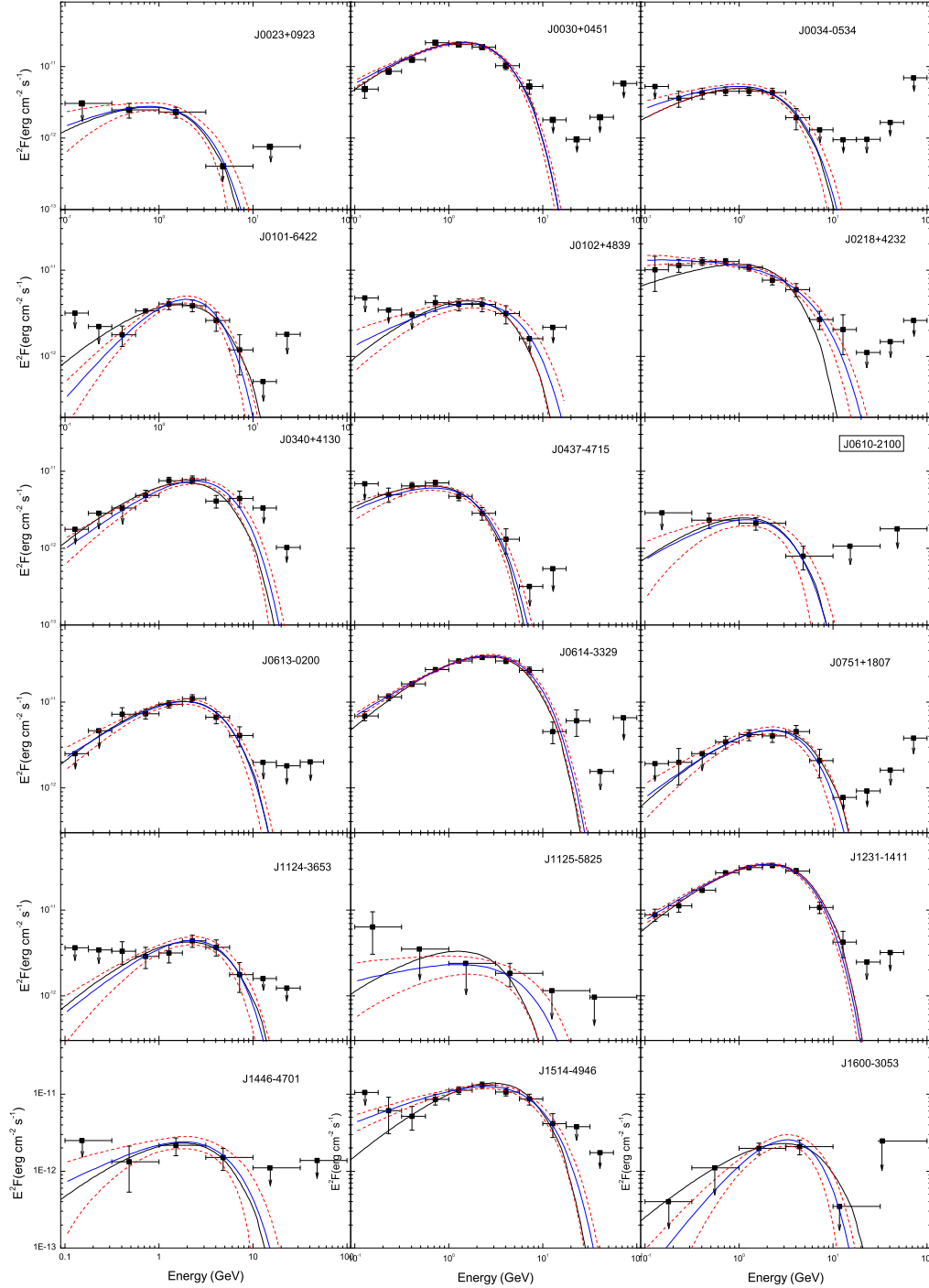


Figure 1. The model results of gamma-ray MSPs. The black solid lines represent the best fitting model spectra with the fitting parameters listed in Table 1. The data points are the observed data from the *Fermi*-LAT, which are taken from Abdo et al. (2013). The best fits (blue lines) with one σ uncertainties (red dashed lines) are also shown by using a power law with an exponential cutoff (Abdo et al. 2013) for comparison.

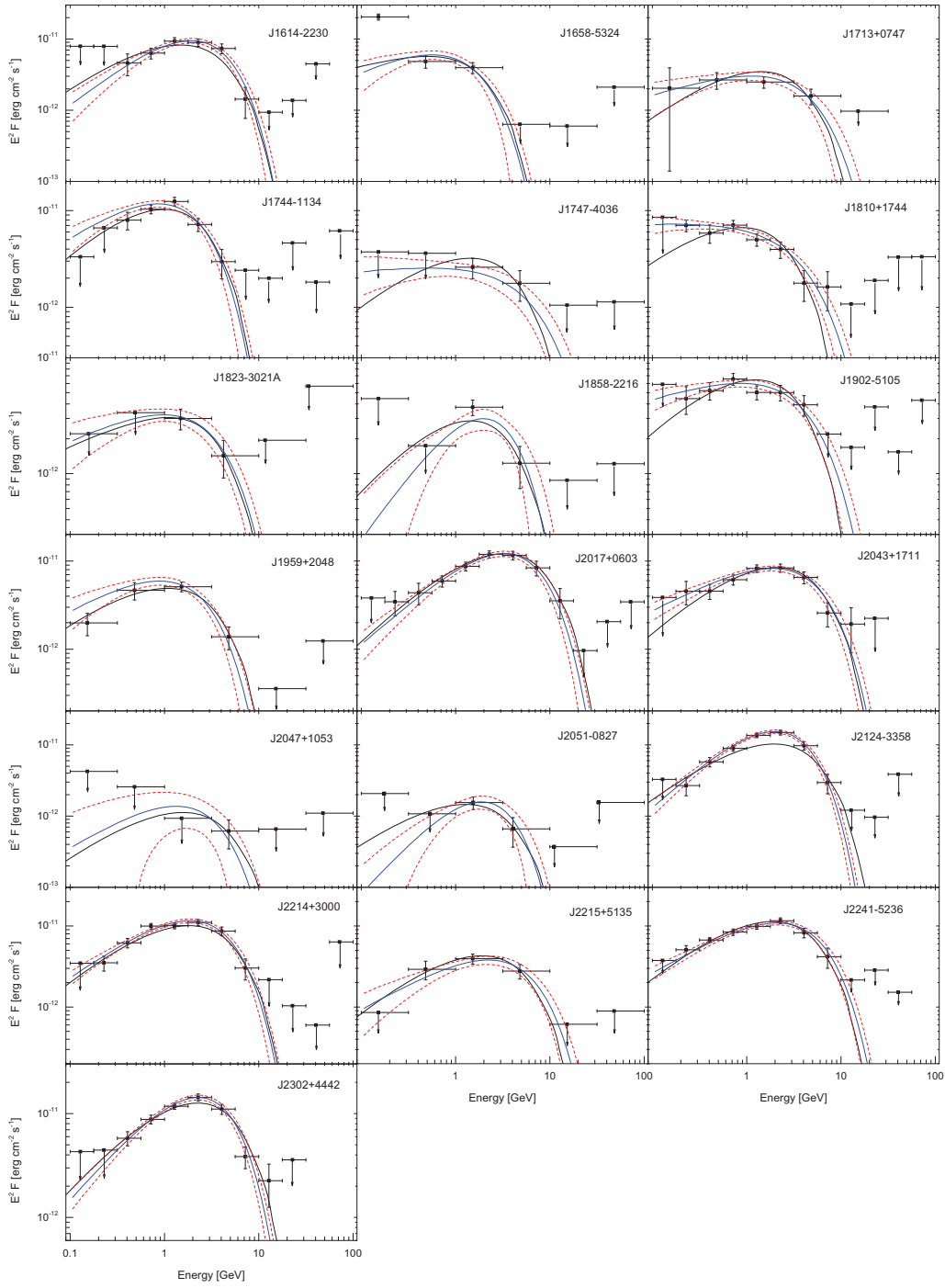


Figure 2. Same as Figure 1.

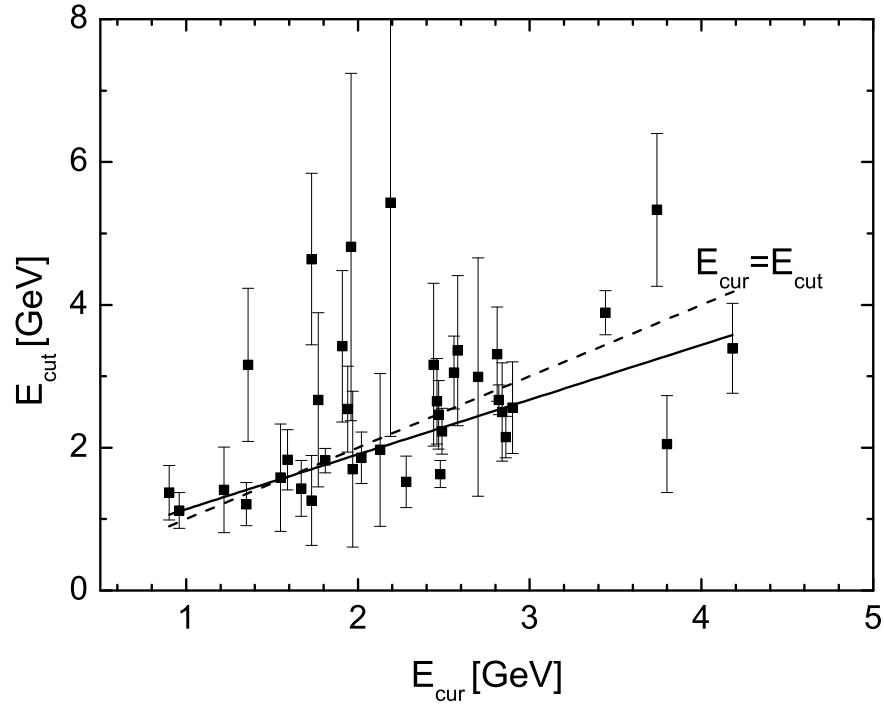


Figure 3. Relation between the observed cutoff energy E_{cut} and the typical gamma-ray energy E_{cur} . The solid line indicate the fitting relation, the dashed line represents $E_{\text{cur}} = E_{\text{cut}}$.

Table 1. Observed quantities and model parameters of MSPs

Name (PSR)	P (ms)	log(<i>B</i>) (G)	Observed Quantities					Model Parameters								
			Dist (kpc)	$T_{m,o}^{(1)}$ (10^6 K)	$T_{m,o}^{(2)}$ (10^6 K)	log(L_X^{ob}) (erg s $^{-1}$)	α (Deg)	f_m	κ	r_a (R_L)	σ_g	$\Delta\phi/\Delta\Omega$	χ/ν	$T_m^{(1)}$ (10^6 K)	$T_m^{(2)}$ (10^6 K)	log(L_X^{th}) (erg s $^{-1}$)
J0023+0923	3.05	8.27	$0.69^{+0.21}_{-0.11}$	–	$2.2^{(a)}$	30.0	48	0.27	1.36	0.80	0.20	0.11	0.12	0.78	2.89	31.00
J0030+0451	4.87	8.35	$0.28^{+0.10}_{-0.06}$	1.18	$2.51^{(b)}$	30.6	58	0.48	1.75	0.85	0.30	0.11	2.81	0.71	2.49	30.70
J0034–0534	1.88	7.99	$0.54^{+0.10}_{-0.10}$	–	$2.2^{(c)}$	29.6	65	0.27	1.32	0.94	0.20	0.09	0.30	0.69	2.34	30.74
J0101–6422	2.57	8.05	$0.55^{+0.09}_{-0.08}$	–	–	–	69	0.39	1.56	0.95	0.25	0.05	0.57	0.65	2.12	30.51
J0102+4839	2.96	8.27	$2.32^{+0.50}_{-0.43}$	–	–	–	73	0.36	1.53	0.97	0.25	0.81	0.21	0.64	2.17	30.48
J0218+4232	2.32	8.63	$2.64^{+1.08}_{-0.64}$	–	$2.9^{(d)}$	31.2	76	0.18	1.20	1.02	0.15	2.77	2.70	0.69	2.67	30.76
J0340+4130	3.30	8.15	$1.73^{+0.30}_{-0.30}$	–	–	–	67	0.45	1.72	0.93	0.30	0.81	3.00	0.71	1.97	30.64
J0437–4715	5.76	8.76	$0.156^{+0.001}_{-0.001}$	0.52	$1.4^{(c)}$	30.5	32	0.28	1.37	0.75	0.20	0.02	0.90	0.86	3.75	31.22
J0610–2100	3.86	8.34	$3.54^{+5.46}_{-1.00}$	–	–	–	53	0.34	1.51	0.83	0.25	1.88	0.82	0.75	2.75	30.88
J0613–0200	3.06	8.24	$0.90^{+0.40}_{-0.20}$	–	–	–	72	0.39	1.58	0.97	0.25	0.27	1.02	0.64	2.15	30.48
J0614–3329	3.15	8.38	$1.90^{+0.44}_{-0.35}$	–	$2.67^{(e)}$	31.6	81	0.41	1.63	1.05	0.25	2.12	1.89	0.56	1.87	30.15
J0751+1807	3.48	8.22	$0.40^{+0.20}_{-0.10}$	–	$1.69^{(f)}$	29.8	72	0.47	1.78	0.97	0.30	0.02	0.31	0.63	2.06	30.41
J1124–3653	2.41	8.08	$1.72^{+0.43}_{-0.36}$	–	$5.2^{(a)}$	31.0	76	0.39	1.58	1.00	0.25	0.34	0.65	0.59	1.92	30.31
J1125–5825	3.10	8.64	$2.62^{+0.36}_{-0.37}$	–	–	–	75	0.25	1.31	1.00	0.20	0.62	39.68	0.68	2.55	30.66
J1231–1411	3.68	8.45	$0.438^{+0.05}_{-0.05}$	–	$2.44^{(e)}$	30.5	76	0.40	1.62	1.00	0.25	0.15	2.47	0.62	2.14	30.40
J1446–4701	2.19	8.17	$1.46^{+0.22}_{-0.22}$	–	–	–	79	0.34	1.43	1.06	0.25	0.11	0.03	0.59	1.93	30.29
J1514–4946	3.59	8.42	$0.94^{+0.12}_{-0.12}$	–	–	–	81	0.46	1.76	1.05	0.30	0.19	5.29	0.56	1.85	30.13
J1600–3053	3.60	8.27	$1.63^{+0.31}_{-0.27}$	–	–	–	78	0.52	1.93	1.02	0.30	0.12	0.09	0.58	1.85	30.19
J1614–2230	3.15	8.25	$0.65^{+0.05}_{-0.05}$	–	$1.5^{(g)}$	30.4	66	0.36	1.52	0.92	0.25	0.15	5.55	0.73	2.15	30.73
J1658–5324	2.44	8.22	$0.93^{+0.11}_{-0.13}$	–	–	–	38	0.20	1.24	0.77	0.15	0.71	63.36	0.83	3.19	31.22
J1713+0747	4.57	8.30	$1.05^{+0.06}_{-0.05}$	–	–	–	57	0.47	1.72	0.85	0.30	0.25	19.26	0.71	2.48	30.71
J1744–1134	4.07	8.29	$0.417^{+0.017}_{-0.017}$	–	$3.31^{(f)}$	29.0	46	0.37	1.53	0.79	0.25	0.16	1.47	0.76	2.81	30.91
J1747–4036	1.65	8.18	$3.39^{+0.76}_{-0.76}$	–	–	–	79	0.24	1.26	1.08	0.20	1.04	16.08	0.61	2.07	30.44
J1810+1744	1.66	7.95	$2.00^{+0.31}_{-0.28}$	–	$4.3^{(a)}$	31.2	62	0.24	1.26	0.93	0.20	1.80	14.18	0.72	2.45	30.85
J1823–3021A	5.44	9.64	$7.60^{+0.40}_{-0.40}$	–	–	–	82	0.16	1.18	1.06	0.15	2.48	0.42	0.71	3.25	30.76
J1858–2216	2.38	7.99	$0.94^{+0.20}_{-0.13}$	–	–	–	65	0.36	1.50	0.93	0.25	0.13	9.54	0.67	2.20	30.61
J1902–5105	1.74	8.10	$1.18^{+0.21}_{-0.21}$	–	–	–	74	0.25	1.28	1.02	0.20	0.36	3.78	0.65	2.20	30.59
J1959+2048	1.61	8.22	$2.49^{+0.16}_{-0.15}$	–	$3.11^{(f)}$	30.9	74	0.19	1.20	1.03	0.20	1.21	3.56	0.67	2.40	30.72
J2017+0603	2.90	8.20	$1.57^{+0.49}_{-0.15}$	–	–	–	82	0.49	1.82	1.06	0.30	0.47	1.28	0.53	1.66	29.98
J2043+1711	2.38	8.07	$1.76^{+0.15}_{-0.32}$	–	–	–	76	0.39	1.57	1.00	0.25	0.72	9.47	0.59	1.92	30.32
J2047+1053	4.29	8.48	$2.05^{+0.32}_{-0.29}$	–	–	–	66	0.39	1.60	0.91	0.25	0.17	53.22	0.72	2.42	30.71
J2051–0827	4.51	8.39	$1.04^{+0.15}_{-0.15}$	–	$2.90^{(h)}$	29.8	53	0.39	1.63	0.82	0.25	0.09	1.71	0.74	2.73	30.84
J2124–3358	4.93	8.51	$0.30^{+0.07}_{-0.05}$	0.5	$2.2^{(c)}$	30.3	67	0.45	1.77	0.91	0.30	0.03	7.27	0.70	2.36	30.64
J2214+3000	3.12	8.34	$1.54^{+0.18}_{-0.18}$	–	$2.90^{(e)}$	30.9	74	0.36	1.53	0.98	0.25	0.65	1.92	0.64	2.18	30.47
J2215+5135	2.61	8.40	$3.01^{+0.33}_{-0.37}$	–	$8.5^{(a)}$	31.9	79	0.30	1.40	1.03	0.25	0.80	1.14	0.61	2.10	30.38
J2241–5236	2.19	8.15	$0.513^{+0.076}_{-0.076}$	0.81	$3.60^{(i)}$	30.0	77	0.32	1.44	1.01	0.25	0.08	0.91	0.60	2.00	30.37
J2302+4442	5.19	8.42	$1.19^{+0.09}_{-0.23}$	–	$3.6^{(j)}$	30.6	68	0.55	2.03	0.92	0.30	0.59	7.27	0.68	2.18	30.55

Note. — The observed quantities and model parameters of MSPs. The first column is the name of the pulsar, the second to seventh column are the observed quantities: periods in millisecond, surface magnetic fields, distances, temperatures of two thermal components and thermal luminosities (if available), respectively. The data of X-ray emission are taken from: (a) Gentile et al. 2013; (b) Bogdanov & Grindlay 2009; (c) Zavlin 2006; (d) Webb et al. 2004; (e) Ransom et al. 2011; (f) Marelli et al. 2012; (g) Pancrazi et al. 2012; (h) Wu et al. 2012; (i) Keith et al. 2011; (j) Takahashi et al. 2012. The eighth to seventeenth column are the model parameters and derived quantities (see text for detail).